INTERNATIONAL JOURNAL FOR NUMERICAL METHODS IN BIOMEDICAL ENGINEERING
*Int. J. Numer. Meth. Biomed. Engng.* 2013; **00**:1–22
Published online in Wiley InterScience (www.interscience.wiley.com). DOI: 10.1002/cnm

# Power-law hereditariness of hierarchical fractal bones

L. Deseri [1,4], M. Di Paola[2], M. Zingales[2,3]*and P. Pollaci[4]

[1] *Center for Nonlinear Analysis and Department of Mathematical Sciences, Carnegie Mellon University, 4811 Frew Street, Pittsburgh, PA 15213-3890, USA*

[2] *Dipartimento di Ingegneria Civile, Ambientale, Aerospaziale e dei Materiali (DICAM), Universitá degli Studi di Palermo, Viale delle Science, Edificio 8, 90100 Palermo, Italy*

[3] *(BM)[2]-Lab, Mediterranean Center of Human Health and Advanced Biotechnologies, Universitá degli Studi di Palermo, Viale delle Science, Edificio 8, 90100 Palermo, Italy*

[4] *Dipartimento di Ingegneria Civile, Ambientale e Meccanica, Universitá degli Studi di Trento, Via Mesiano 77, 38123 Trento, Italy*

SUMMARY

In this paper the authors introduce a hierarchic fractal model to describe bone hereditariness. Indeed, experimental data of stress relaxation or creep functions obtained by compressive/tensile tests have been proved to be fit by power-law with real exponent $0 \leq \beta \leq 1$. The rheological behavior of the material has therefore been obtained, using the Boltzmann-Volterra superposition principle, in terms of real order integrals and derivatives (fractional-order calculus). It is shown that the power-laws describing creep/relaxation of bone tissue may be obtained introducing a fractal description of bone cross-section and the Hausdorff dimension of the fractal geometry is then related to the exponent of the power-law.


Received . . .

KEY WORDS: Bone Hereditariness; Fractional Calculus; Hierachic Structure, Mechanical Fractance, Power-Law.

## 1. INTRODUCTION

Mathematical models of material behavior are fundamental for optimization and for reliable design of engineered devices. Furthermore, the key issue is to be able to track down the multiscale behavior from the nano- to the macrolevel, with particular regard to biological and bioinspired materials. Indeed, the mechanical interactions among biomedical devices and biological tissues play a key-role for the optimization of physiological functionality of such devices owing to the reduction of immunologic response. In this regard, it is clear that the detailed knowledge of the features of biological tissues at the different scales and their interactions with the devices is a crucial step to optimize the mechanical and physical response of the compound.

Physical parameters of biological tissues usually investigated in scientific literature involve stiffness, strength, toughness, permeability, porosity, thermal conductivity among others [1, 2, 3]. Besides these important features, mineralized bone tissues must provide load carrying capabilities and they exhibit a marked time-dependent behavior under applied loads. In this context, the term *hereditariness* is usually used in the sense that the actual response of bone material in terms of

*Correspondence to: Journals Production Department, John Wiley & Sons, Ltd, The Atrium, Southern Gate, Chichester, West Sussex, PO19 8SQ, UK.

stress/displacement depends on previously applied stress/strain. This feature is macroscopically detectable by stress relaxation and creep observed in classical traction/compression mechanical tests. During a relaxation test, the imposed strain is held constant and a measure of the stress is monitored showing that it is a decreasing function of time; similarly, in a creep test an imposed constant stress is applied and a continuous monitoring of the strain is considered showing that it is an increasing function of time. Both these tests highlight the hereditariness feature of such material; the past undergone stress or strain history influence the future response of the specimen. A similar time-dependent behavior also arises in mineralized tissues as ligaments and tendons. Indeed the high stiffness (but highly brittleness) of the hydroxyapatite crystals in these tissues is combined with the high ductility of the collagen proteic matrix. In this way a stiffer nano-structured with composite material is obtained that possesses high strength [4] with time-dependent behavior set on a multiple time scales from pico to nano seconds [5, 6, 7]. The hereditariness of the mineralized collagen matrix is detected at various observation scales where different arrangements of the basic elements of the material structure are observed [8, 9, 10]. The bone specimen cross-section assembly exhibits a fractal-like structure. This yields anomalous scaling of stiffness and viscosity coefficients and it constitutes a mechanical hierarchy dubbed *fractance*, in close relation with fractal geometry. In this regard the material structure forms a hierarchy that yields exceptional features at the macroscale in terms of strength, stiffness and toughness. Moreover, the hierarchical assembly, composed by hydroxyapatite and collagen, justifies the presence of both several relaxation times (strictly related to inner microstructure) and anisotropy, well highlighted through specific mechanical tests such as the three-point bending [11].

In this study the authors will show that relaxation/creep functions of trabecular and compact bones are well captured by real-order power-laws $t^\beta$ $(0 < \beta \leq 1/2)$ yielding a rheological model in term of real-order differintegral operators [12, 13, 14]. The presence of a power-law with $0 < \beta \leq 1/2$ has been justified with a mechanical model represented by a Newtonian viscous material resting on a bed of independent spring [15]. The presence of such mechanical model, however, is not observed in bone tissue and, in this paper, a fractal description of bone cross-section will be introduced. In this regard it will be shown that the specimen cross-section at any level of hierarchy has a non-Euclidean dimension. As we assume that this dimension is identical at several observation scale of the bone, as in fractal set, a relation among the the power-law and the fractal dimension exists.

In the next section we discuss the macroscopic hereditariness and the corresponding rheological model in terms of fractional-order operators. Sections 3 and 4 are devoted to the mechanical analogues of fractional-order elements. The fractance description of bone self-assembly hierarchy leading to macroscale hereditariness is introduced in Section 5, whereas some conclusions are drawn in Section 6. Additionally some appendices involving the basic concepts of fractional-order calculus, fractal geometry and continued fraction algebra have been reported.

## 2. BONE HEREDITARINESS: THE POWER-LAW RHEOLOGICAL MODEL

Mineralized biological tissues as bones, tendons and ligaments are very sophisticated and highly specialized engineered materials. Macroscopic observations of trabecular bone tissue show that its architecture is built upon a complex network of beams and platelets forming a three-dimensional geometric structure. Spaces among the mineralized tissues are filled by bone marrow, a fluid-like material formed by fat cells, water and proteins. The biphasic nature of the trabecular bone is the main reason why its macroscopic mechanical behavior fades out stress peaks due to high frequency and impulsive loads. Mathematical models of the macroscopic behavior of biphasic trabecular bones make wide use of the Biot's poroelasticity [16, 17, 18, 19, 20], although a more modern treatment of such media may be found through the theory of Structured Deformations [21, 22, 23].

Despite the macroscopic behavior of trabecular bones, the rheological description of mineralized biological tissues deserves careful considerations. Indeed load capacity and ultimate strength of bones, as well as stiffness, depend on the mechanical properties of the solid-like phase. However several pathological diseases such as osteoporosis and/or osteosynthesis affect, specifically, the nano-micro scale structure of the mineralized tissue modifying, primarily, its rheological properties



DOI: 10.1002/cnm

[24, 25, 26]. In this regard, it is well known that the structure of bones is self-organized in a hierarchic sequence repeating its fundamental elements in different stacking at different resolution scales [8].

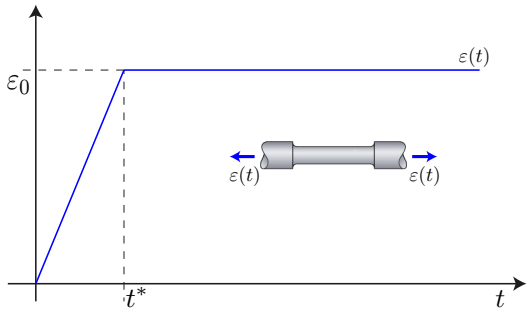


Figure 1. Schematic representation of relaxation test: after the initial ramp, the strain is held constant.

The overall behavior of the mineralized tissue is detected through macroscale relaxation tests from several authors [27, 28, 29] and is displayed in Figure 2. In the pictures, the dots represent the experimental data whereas solid lines are the fitting relaxation curves chosen in the following class:

$$G(t) := \frac{C_\beta}{\Gamma(1-\beta)} t^{-\beta} \qquad \beta \in [0,1] \tag{1}$$

where $G(t)$ and $\Gamma(1-\beta)$ are the relaxation function and the Euler-Gamma function evaluated at $t$ and at $1-\beta$ respectively and $[C_\beta] = FT^\beta/L^2$ is an anomalous *force* coefficient of the material. Inspection of Figure 2 shows that the fitting curves in (1) are in good agreement with experimental results for different kinds of bones undergoing to relaxation tests (schematically represented in Figure 1). The viscoelastic behavior of collagen is then shown to agree with our choice of the class of relaxation functions, even if a closer analysis of data seems to require an additional constant elastic term to model the equilibrium response. Indeed, the hereditary feature causes continuum stress relaxation in time depending on an exponent near to 0 (see Table I). Henceforth the stress value fades out in a very long time. Experimental tests are performed in a limited time frame, so that the proposed model approximates very well the experimental data in the given time-range [30, 31, 32]. The results of best-fitting procedure, collected in Table I, show that the power-law exponent depends on the anatomical location of the considered specimen [33]. This observation is in good agreement with several bone microscopies showing that the mineralized tissue architecture changes upon the anatomic location as the result of a material optimization procedure. In the context of linear hereditariness and in the absence of past histories, the Boltzmann-Volterra superposition principle may be used to provide the stress response as well as the strain evolution for prescribed strain $\gamma$ (stress $\sigma$) processes:

$$\sigma(t) := \int_0^t G(t-\tau)\dot{\gamma}(\tau)d\tau \tag{2a}$$

$$\gamma(t) := \int_0^t J(t-\tau)\dot{\sigma}(\tau)d\tau. \tag{2b}$$

As the model parameters have been obtained from the best-fitting of experimental data on stress relaxations, the creep function $J(t)$ may be obtained from the relaxation function $G(t)$ in (1) by mean of the well-known relation in the Laplace domain, i.e.

$$\tilde{G}(s)\tilde{J}(s) = \frac{1}{s^2} \quad \Longrightarrow \quad J(t) = \frac{1}{C_\beta \Gamma(1+\beta)} t^\beta \tag{3}$$

where the symbol $\tilde{}$ denotes the Laplace transform. By inspection of the last term in the equality



DOI: 10.1002/cnm

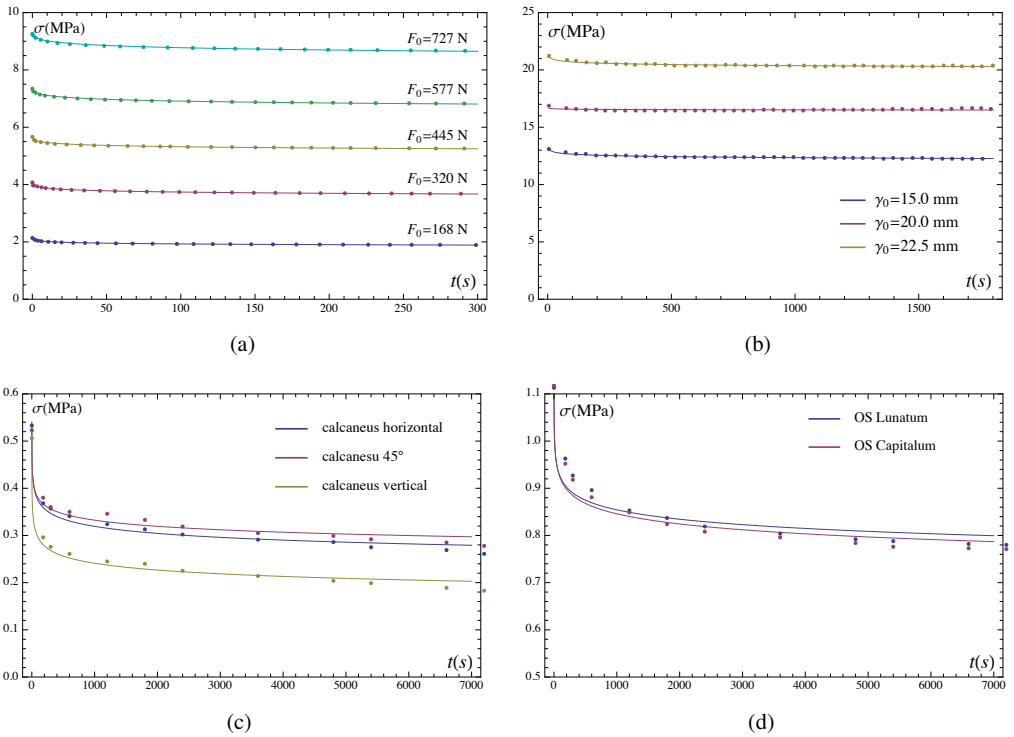


Figure 2. Fitting of relaxation experimental data from several authors: a) [27]; b) [29]; c) and d) [28].

Table I. Parameters from best-fitting procedure on curve in Figure 2.

| | | $\beta$ | $C_\beta \left[\frac{N}{mm^2} s^\beta\right]$ | Notes |
|---|---|---|---|---|
| (a) [27] | $F_0 = 168\ N$ | 0.0194 | 71.17 | bovine femural head |
| | $F_0 = 320\ N$ | 0.0171 | 71.52 | |
| | $F_0 = 445\ N$ | 0.0128 | 71.58 | |
| | $F_0 = 577\ N$ | 0.0139 | 72.13 | |
| | $F_0 = 727\ N$ | 0.0136 | 72.56 | |
| (b) [29] | $\varepsilon_0 = 1.143\%$ | 0.0690 | 46.99 | human calcaneus horizontal |
| | $\varepsilon_0 = 0.678\%$ | 0.0575 | 75.61 | human calcaneus 45° |
| | $\varepsilon_0 = 0.478\%$ | 0.0886 | 98.53 | human calcaneus vertical |
| | $\varepsilon_0 = 0.480\%$ | 0.0341 | 229.95 | os lunatum |
| | $\varepsilon_0 = 0.707\%$ | 0.0372 | 158.22 | os capitalum |
| (c) [28] | $u_0 = 0.15\ mm$ | 0.0104 | 88.99 | bovine femur |
| | $u_0 = 0.20\ mm$ | 0.0015 | 83.50 | |
| | $u_0 = 0.25\ mm$ | 0.0069 | 84.09 | |

chains in (2) through the definitions reported in Appendix A, it is shown that assuming a power-law expression of the relaxation/creep function of the material results into rheological expressions:

$$\sigma(t) = \frac{C_\beta}{\Gamma(1-\beta)} \int_0^t (t-\tau)^{-\beta} \dot{\gamma}(\tau) d\tau = C_\beta \left( {}_C\mathrm{D}^\beta_{0+} \gamma \right)(t) \tag{4a}$$

$$\gamma(t) = \frac{1}{C_\beta \Gamma(1+\beta)} \int_0^t (t-\tau)^{\beta} \dot{\sigma}(\tau) d\tau = \frac{1}{C_\beta} \left( \mathrm{I}^\beta_{0+} \sigma \right)(t) \tag{4b}$$



DOI: 10.1002/cnm

containing the well-known Caputo and Riemann-Liouville differential and integral operators. For “non-virgin" materials, i.e. materials whose state at the very beginning of observation is characterized by prestressed (or prestrained) configuration, equation (2) would be supplemented by state variables [34, 35, 36]. The use of fractional operators in the context of rheological material modeling has been proved to be a key tool to predict the hereditariness of stresses and strains in organic polymers [37, 38, 39]. The rheological description of the hereditary features of bone tissues has been shown in Figure 2, where the material parameters have been estimated by a best fitting procedure for different kinds of trabecular bone tissues. The stress-strain behavior in (4) may be fruitfully explained by making use of a rheological device, called *springpot* [40]. The springpot has an intermediate behavior between a linear spring, whose constitutive equations reads as $\sigma = E\gamma$, and a Newtonian dashpot with constitutive law relation $\sigma = \eta\dot{\gamma}$ (Figure 3). Limiting values of the

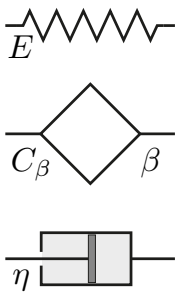


$$\sigma(t) = E(\mathrm{D}^0\gamma)(t) = E\gamma(t) \qquad (\beta = 0)$$

$$\sigma(t) = C_\beta(\mathrm{D}^\beta\gamma)(t) \qquad (0 < \beta < 1)$$

$$\sigma(t) = \eta(\mathrm{D}^1\gamma)(t) = \eta\dot{\gamma}(t) \qquad (\beta = 1)$$

Figure 3. The mechanical *devices*: (a) spring, (b) springpot, (c) dashpot.

order of differentiation $\beta \to 0$ or $\beta \to 1$ yield springs and dashpot devices, respectively. The fairly limited use of fractional-order derivatives in the context of mechanics is related to the lack of a clear mechanical description of the associated rheological devices. An efficient and exact representation of springpot devices has been recently obtained [15, 41] and it will be called in the next section.

## 3. THE MECHANICAL MODEL OF BONE FRACTIONAL-ORDER HEREDITARINESS

An exact mechanical model of fractional hereditary materials was recently proposed in [15], where two different mechanical representations of fractional hereditary material (FHM) depending on the mathematical range of the exponent $\beta$ are reported. The mechanical description of *Elasto-Viscous* (EV) materials ($0 \le \beta \le 1/2$) is represented by an indefinite massless viscous shear fluid externally restrained by a bed of independent elastic springs. *Visco-Elastic* (VE) materials ($1/2 \le \beta \le 1$) are represented instead by an indefinite elastic shear layer externally restrained by independent linear dashpots (Figure 4).

We assume that the mechanical parameters of the model, namely the elastic modulus $k(z)$ and the viscosity coefficient $c(z)$ decay with power-law with the axial coordinate $z$ as:

$$k_{E}(z) := AG_{E}(z) = A\frac{G_0}{\Gamma(1+\alpha)}z^{-\alpha} \tag{5a}$$

$$c_{E}(z) := A\eta_{E}(z) = A\frac{\eta_0}{\Gamma(1-\alpha)}z^{-\alpha}, \tag{5b}$$

for EV materials (denoted by subscript $E$), whereas for VE materials (denoted by subscript $V$) they read as follows:

$$k_{V}(z) := AG_{V}(z) = A\frac{G_0}{\Gamma(1-\alpha)}z^{-\alpha} \tag{6a}$$

$$c_{V}(z) := A\eta_{V}(z) = A\frac{\eta_0}{\Gamma(1+\alpha)}z^{-\alpha} \tag{6b}$$



DOI: 10.1002/cnm

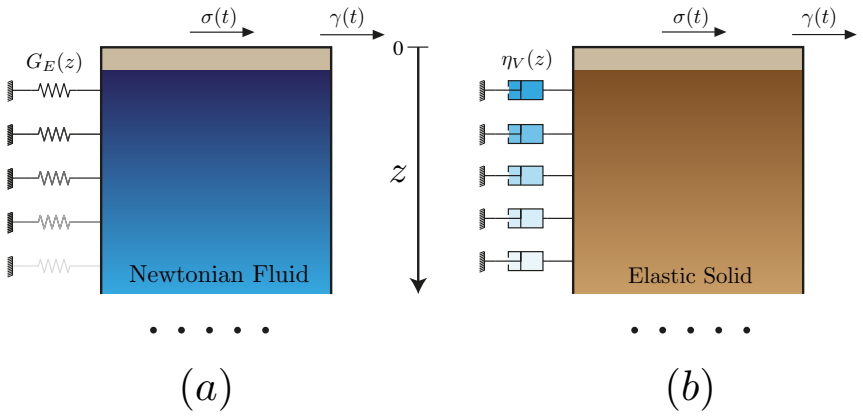


Figure 4. Continuum fractional models: (a) elastoviscous (EV) and (b) viscoelastic (VE) cases.

where $0 \leq \alpha \leq 1$, $A$ is the cross-sectional area and $G_{_E}, G_{_V}$ and $\eta_{_E}, \eta_{_V}$ represent the elastic modulus and the viscosity coefficient per unit of area for both cases respectively (see [15] for more details). In the following we assume a unit area ($A = 1$) so that $k_{_{E,V}}(z) = G_{_{E,V}}(z)A = G_{_{E,V}}(z)$ and $c_{_{E,V}}(z) = \eta_{_{E,V}}(z)A = \eta_{_{E,V}}(z)$. In these circumstances the balance of linear momentum of the model reads:

$$(\text{EV}): \quad \frac{\partial}{\partial z}\left[c_{_E}(z)\frac{\partial \dot{\gamma}}{\partial z}\right] = k_{_E}(z)\gamma(z,t) \tag{7a}$$

$$(\text{VE}): \quad \frac{\partial}{\partial z}\left[k_{_V}(z)\frac{\partial \gamma}{\partial z}\right] = c_{_V}(z)\dot{\gamma}(z,t), \tag{7b}$$

where $\gamma(z,t)$ is the transverse displacement of the shear layer at depth $z$ and $\dot{\gamma}(z,t) = \frac{\partial \gamma(z,t)}{\partial t}$ Boundary conditions associated to the mechanical model in Figure 4 are provided in the form:

$$\begin{cases} \lim\limits_{z\to 0} \gamma(z,t) = \gamma(t) \\ \lim\limits_{z\to \infty} \gamma(z,t) = 0. \end{cases} \tag{8}$$

Upon solving the boundary value problem, the stress arising at the top surface turns out to be related to the transverse displacement $\gamma(t)$ by the following relation:

$$\sigma(t) = C_\beta \left({}_C\mathrm{D}^{\beta}_{0+}\gamma\right)(t)\,, \tag{9}$$

where:

$$C_\beta := C^{E}_{\beta} = \frac{G_0\Gamma(\beta)}{\Gamma(2-2\beta)\Gamma(1-\beta)2^{1-2\beta}}\left(\tau_{_E}(\alpha)\right)^{\beta} \tag{10a}$$

$$\tau_{_E}(\alpha) = -\frac{\eta_0}{G_0}\frac{\Gamma(\alpha)}{\Gamma(-\alpha)} \tag{10b}$$

and $\alpha = 1 - 2\beta$ for the EV material, whereas:

$$C_\beta := C^{V}_{\beta} = \frac{G_0\Gamma(1-\beta)}{\Gamma(2-2\beta)\Gamma(\beta)2^{2\beta-1}}\left(\tau_{_V}(\alpha)\right)^{\beta} \tag{11a}$$

$$\tau_{_V}(\alpha) = -\frac{\eta_0}{G_0}\frac{\Gamma(-\alpha)}{\Gamma(\alpha)} \tag{11b}$$

and $\alpha = 2\beta - 1$ for the VE material, where the terms $\tau_{_E}(\alpha)$, $\tau_{_V}(\alpha)$ are dimensionally a relaxation time. This result shows that the mechanical models analyzed above and formed by a proper



DOI: 10.1002/cnm

arrangement of springs and dashpots with mechanical parameters decaying with power-law provides exactly a rheological model in terms of fractional derivatives.

It is worth noting, with the aid of the normalized creep function $\overline{J}(t) = J(t)C_\beta\Gamma(1+\beta) = t^\beta$ (see Figure 5), that the value $\beta = 1/2$ of the derivation order separates two different ranges for the material behavior. In the range $1/2 \leq \beta \leq 1$ the viscosity prevails, the elastic phase decreases with increasing $\beta$ and then it is appropriate to define such materials as VE. The corresponding mechanical model is composed by an elastic indefinite column undergoing shearing and resting on a bed of linear dashpots. The second behavior is characterized by $0 \leq \beta \leq 1/2$ in which the elastic phase prevails with decreasing $\beta$, and then it is appropriate to define these materials as EVs. The corresponding mechanical model is described as an unbounded column of viscous fluid resting on a bed of linearly independent springs.

The critical value of the fractional derivation order $\beta = 1/2$ may be also obtained as a limit case for the two different models described above.

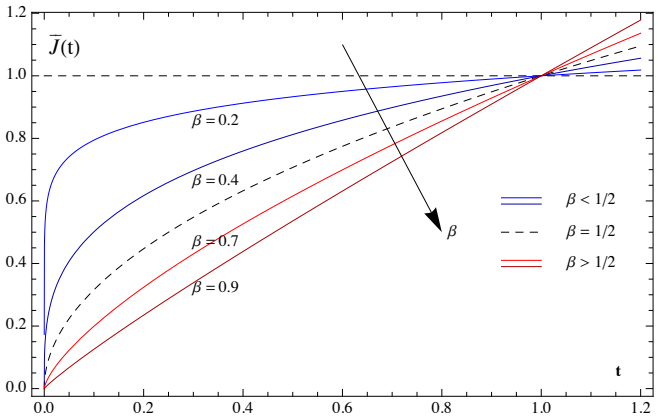


Figure 5. Normalized creep function $\overline{J}(t)$ (curves with different $\beta$).

## 4. THE DISCRETE EQUIVALENT REPRESENTATION OF FHM

Validation and challenges of the mechanical equivalent representation of FHM have been discussed in previous papers [42, 41] for EV ($0 \leq \beta \leq 1/2$) and VE ($1/2 \leq \beta \leq 1$) materials. To this aim the continuum mechanical model has been discretized into a mechanical fractance. Introducing a finite discretization grid of the $z-$axis into point $z_j = (j-1)\Delta z,\ j = 1, 2, \ldots, n$, with step $\Delta z = h/n$ where $h$ is the spatial extension of the fractance.

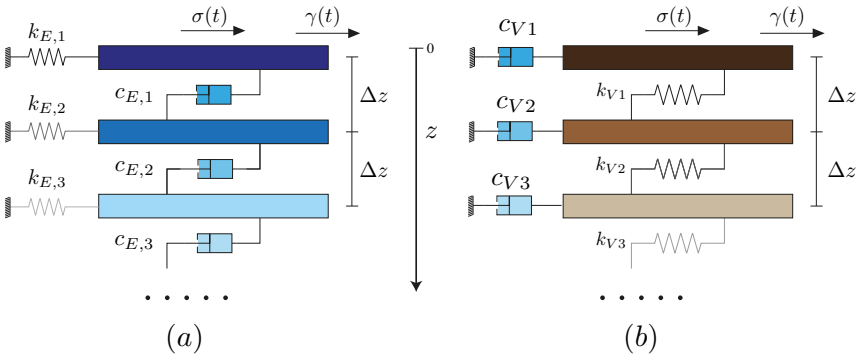


Figure 6. Fractional mechanical model: discrete counterpart of (a) EV and (b) VE materials.



DOI: 10.1002/cnm

The introduction of $z-$axis discretization yields discrete mechanical fractances both for EV and VE cases (Figure 6) with stiffness and damping coefficients that for EV case read:

$$k_{E,j} = G_E(j\Delta z)\Delta z = \frac{\eta_0}{\Gamma(1+\alpha)}\,(j\Delta z)^{-\alpha}\;\Delta z \tag{12a}$$

$$c_{E,j} = \frac{\eta_E(j\Delta z)}{\Delta z} = \frac{G_0}{\Gamma(1-\alpha)}\frac{(j\Delta z)^{-\alpha}}{\Delta z}. \tag{12b}$$

Hence, the equilibrium equations are provided in the following form:

$$\begin{cases} \sigma(t) = k_0\gamma_1 - c_0\Delta\dot{\gamma}_0 \\ k_j\gamma_j - c_j\Delta\dot{\gamma}_j + c_{j-1}\Delta\dot{\gamma}_{j-1} = 0 \end{cases} \tag{13}$$

where $\Delta\dot{\gamma}_{j+1} = \dot{\gamma}_{j+1} - \dot{\gamma}_j$. May be shown that as $\Delta z \to 0$ and $h \to \infty$ (13) reverts to the governing equation in (7b). Similar considerations hold for VE models as we select the spring coefficient of the model in (6b) as follows:

$$k_{V,j} = \frac{G_V(z)}{\Delta z} = \frac{G_0}{\Gamma(1-\alpha)}j^{-\alpha}\frac{\Delta z^{-\alpha}}{\Delta z} \tag{14a}$$

$$c_{V,j} = \eta_V(z)\Delta z = \frac{\eta_0}{\Gamma(1+\alpha)}j^{-\alpha}\Delta z^{-\alpha}\;\Delta z, \tag{14b}$$

while the equilibrium equation are:

$$\begin{cases} \sigma(t) = c_0\dot{\gamma}_0 - k_0\Delta\gamma_1 \\ c_j\dot{\gamma} - k_j\Delta\gamma_j + k_{j-1}\Delta\gamma_{j-1} = 0 \end{cases} \tag{15}$$

where $\Delta\gamma_{j+1} = \gamma_{j+1} - \gamma_j$.

The discretized version of the equilibrium equations may be cast in a compact form for EV and VE, namely:

$$p_E\mathbf{A}\dot{\boldsymbol{\gamma}} + q_E\mathbf{B}\boldsymbol{\gamma} = \mathbf{v}\sigma(t) \tag{16a}$$

$$p_V\mathbf{B}\dot{\boldsymbol{\gamma}} + q_V\mathbf{A}\boldsymbol{\gamma} = \mathbf{v}\sigma(t), \tag{16b}$$

where $p$ and $q$ are constant coefficients only depending on discretization increment $\Delta z$, $\boldsymbol{\gamma}$ is the vector of displacement at each layer of discretization, $\mathbf{v}\sigma(t)$ is the vector of applied stress, and:

$$p_E := \frac{\eta_0}{\Gamma(1-\alpha)}\Delta z^{-(1+\alpha)} \qquad p_V := \frac{\eta_0}{\Gamma(1+\alpha)}\Delta z^{1-\alpha} \tag{17a}$$

$$q_E := \frac{G_0}{\Gamma(1+\alpha)}\Delta z^{1-\alpha} \qquad q_V := \frac{G_0}{\Gamma(1-\alpha)}\Delta z^{-(1+\alpha)} \tag{17b}$$

$$\boldsymbol{\gamma} = [\gamma_1 \quad \gamma_2 \ldots \gamma_n]^T \qquad \mathbf{v} = [1 \quad 0 \ldots 0]^T, \tag{17c}$$

Here the matrices $\mathbf{A}$ and $\mathbf{B}$ are defined as follows:

$$\mathbf{A}_{i,j} = \begin{cases} (i-1)^{-\alpha} + i^{-\alpha} & i = j \\ -i^{-\alpha} & (j-i) = 1 \text{ with } j > i \\ -j^{-\alpha} & (i-j) = 1 \text{ with } i > j \\ 0 & other \end{cases}$$

$$\mathbf{A} = \begin{bmatrix} 1^{-\alpha} & -1^{-\alpha} & 0 & \ldots & 0 \\ 1^{-\alpha} & 1^{-\alpha} + 2^{-\alpha} & 2^{-\alpha} & \ldots & 0 \\ 0 & 2^{-\alpha} & 2^{-\alpha} + 3^{-\alpha} & \ldots & 0 \\ \vdots & \vdots & \vdots & \ddots & \vdots \\ 0 & 0 & 0 & \ldots & (n-1)^{-\alpha} + n^{-\alpha} \end{bmatrix} \tag{18}$$



DOI: 10.1002/cnm

$$\mathbf{B}_{i,j} = \begin{cases} i^{-\alpha}, & i = j \\ 0, & i \neq j \end{cases}$$

$$\mathbf{B} = \begin{bmatrix} 1^{-\alpha} & 0 & 0 & \dots & 0 \\ 0 & 2^{-\alpha} & 0 & \dots & 0 \\ 0 & 0 & 3^{-\alpha} & \dots & 0 \\ \vdots & \vdots & \vdots & \ddots & \vdots \\ 0 & 0 & 0 & \dots & n^{-\alpha} \end{bmatrix} \tag{19}$$

We note that $\mathbf{B}$ is actually positive difinite and, hence, invertible. In the sequel we will report analysis and solutions for both elastoviscous and viscoelastic materials.

We now focus our attention on EV case. The solution of the system of differential equations in (16a) will be obtained introducing the following change of coordinate:

$$\mathbf{x} = \mathbf{B}^{\frac{1}{2}}\boldsymbol{\gamma} \tag{20}$$

By left-multiplying both sides of (16a) by $\mathbf{B}^{-\frac{1}{2}}$, we obtain:

$$p_E\mathbf{D}\dot{\mathbf{x}} + q_E\mathbf{I}\mathbf{x} = \mathbf{B}^{\frac{1}{2}}\mathbf{v}\sigma(t), \tag{21}$$

where $\mathbf{D} = \mathbf{B}^{-\frac{1}{2}}\mathbf{A}\mathbf{B}^{-\frac{1}{2}}$ is the dynamical matrix, and it is symmetric and positive and $\mathbf{I}$ is the identity operator. This equation my be studied making use of $\boldsymbol{\Phi}$ (where each column is an eigenvector of $\mathbf{D}$ ), which has the following properties:

$$\boldsymbol{\Phi}^T\mathbf{D}\boldsymbol{\Phi} = \boldsymbol{\Lambda} \tag{22a}$$

$$\boldsymbol{\Phi}^T\boldsymbol{\Phi} = \mathbf{I}, \tag{22b}$$

where $\boldsymbol{\Lambda}$ is the diagonal matrix of the eigenvalues $\lambda_i > 0$ of $\mathbf{D}$. In order to obtain a decoupled set of equations, the modal transformation $\mathbf{x} = \boldsymbol{\Phi}\,\mathbf{y}$ is performed; henceforth by left-multiplicating for $\boldsymbol{\Phi}^{-1} = \boldsymbol{\Phi}^T$, the following modal equation arises:

$$p_E\boldsymbol{\Lambda}\dot{\mathbf{y}} + q_E\mathbf{y} = \boldsymbol{\Phi}^T\mathbf{v}\,\sigma(t) \tag{23}$$

where $\mathbf{B}^{\frac{1}{2}}\mathbf{v} = \mathbf{v}$ for the special form both of $\mathbf{B}$ and $\mathbf{v}$.

Following the same steps with the same assumptions the governing equation for VE discrete model read as follows:

$$p_V\dot{\mathbf{y}} + q_V\boldsymbol{\Lambda}\mathbf{y} = \boldsymbol{\Phi}^T\mathbf{v}\,\sigma(t). \tag{24}$$

In the modal space, the $j^{th}$ equation of each model takes the following form:

$$\dot{y}_j + \frac{q_E}{p_E\lambda_j}y_j = \frac{\phi_{1,j}}{p_E\lambda_j}\sigma(t) \tag{25a}$$

$$\frac{p_V}{q_V\lambda_j}\dot{y}_j + y_j = \frac{\phi_{1,j}}{q_V\lambda_j}\sigma(t), \tag{25b}$$

where $\phi_{1,j}$ is the first element of the $j^{th}$ eigenvector of the dynamical matrix $\mathbf{D}$. Equations (25) are analog to the ones governing the evolution of a generic Kelvin-Voigt element with viscous coefficient $a_E := 1$ ($a_V := p_V/(q_V\lambda_j)$, elastic spring $b_E := q_E/(p_E\lambda_j) > 0$ ($b_V := 1$), and forced by $\sigma_j := f_j\sigma(t)$ :

$$a_j\dot{y}_j + b_j\,y_j = f_j\sigma(t) \quad j = 1,\,2,\dots,\,n; \tag{26}$$

the previous statement allows for detecting the relaxation time of each level as the ratio $\tau_j = b_j/a_j$. In equation (26) the magnitude modal-load coefficients are defined as follows:

$$f_j := \begin{cases} f_E = \dfrac{\phi_{1,j}}{p_E\lambda_j} & \text{EV} \\ f_V = \dfrac{\phi_{1,j}}{q_V\lambda_j} & \text{VE} \end{cases}. \tag{27}$$



DOI: 10.1002/cnm

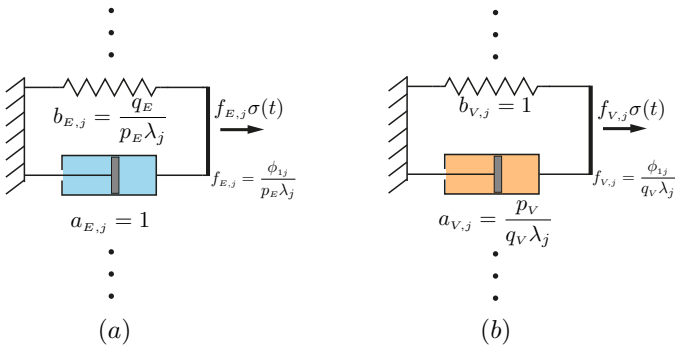


Figure 7. The $j^{th}$ EV (a) and VE (b) Kelvin-Voigt resolution model in modal space.

Setting the initial condition properly as

$$\mathbf{y}(0) = \mathbf{\Phi}^T \mathbf{B}^{\frac{1}{2}} \boldsymbol{\gamma}(0) \tag{28}$$

the complete solution of differential equation of Kelvin-Voigt model in the modal space reads:

$$y(t) = y_j(0) \mathrm{e}^{-\frac{b_j}{a_j} t} + \frac{f_j}{a_j} \int_0^t \mathrm{e}^{-\frac{b_j}{a_j}(t-\tau)} \sigma(\tau) d\tau, \tag{29}$$

where $y_j(0)$ is the $j^{th}$ element of initial values vector $\mathbf{y}(0)$; yielding the displacement vector of the fractance as:

$$\boldsymbol{\gamma}(t) = \mathbf{B}^{-\frac{1}{2}} \mathbf{\Phi} \mathbf{y}(t). \tag{30}$$

The displacement at the top of the mechanical model is provided by the first element of the solution vector $\boldsymbol{\gamma}(t)$. In order to separate such a displacement from the rest of the response, one can make use of the vector $\mathbf{v}$ defined before, i.e. $\gamma(t) = \mathbf{v}^T \boldsymbol{\gamma}(t)$.

Inspection of (25) shows that the dynamical system in the modal space is described by a set of decoupled, linear, one-degree of freedom system with different relaxation times $\tau_j$. Such a consideration shows that the continuous spectrum relaxation function of FHM may be properly discretized in a set of spectral rows corresponding to relaxation times $\tau_j$, $(j = 1, 2, \dots, n, \dots)$.

The capability of the model may be shown for EV and VE forced by a constant force $\sigma(t) = \sigma_0 = U(t)$. The solution of generic Kelvin-Voigt for a quiescent system at its starting time (i.e. the initial conditions are zero for each layer) in modal space reads as follows:

$$y_j(t) = f_j \sigma_0 \left( 1 - \mathrm{e}^{-\frac{b_j}{a_j} t} \right)$$

In particular, Figure 8a shows the influence of the number of layer $n$ (using $\beta = 0.4$ and $\Delta z = 0.001$). Figure 8b shows the influence of $\Delta z$ (using $\beta = 0.4$ and $n = 500$). It may be observed that as soon as more layers are considered the solution converges towards the exact expression of a fractional integral. At last, the exact and discrete solutions are compared for several values of $\beta$ studying both EV case ($n = 1500$, $\Delta z = 0.001$) and VE case ($n = 1500$, $\Delta z = 0.02$), as depicted in Figure 8c and Figure 8d respectively. It is interesting to note that the predicted response for VE needs a lower discretization step to match the exact one.

We may summarize our analysis by recalling that we showed that the mechanical model yields a power-law creep function and that the discretized model involves a discretized time spectrum. In this regard we may consider that FHM as a continuum counterpart of 1D linearly independent $n$ degree of freedom system with decaying stiffness and viscosity. This behavior will be used in Section 5 to address bone hereditary response.



DOI: 10.1002/cnm

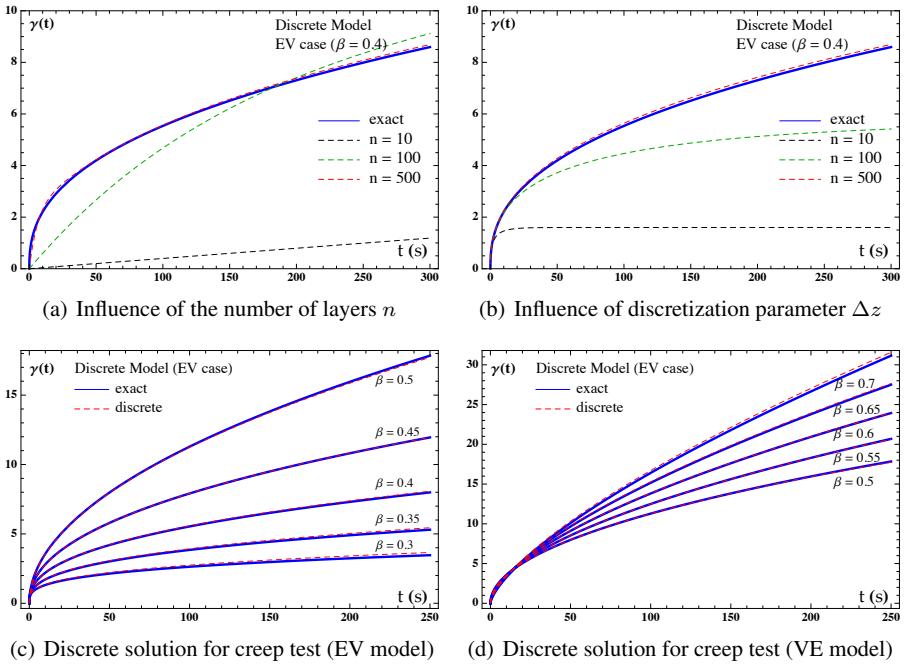


(a) Influence of the number of layers $n$ (b) Influence of discretization parameter $\Delta z$

(c) Discrete solution for creep test (EV model) (d) Discrete solution for creep test (VE model)

Figure 8. The influence of parameters on discrete solution and its match with exact values for several values of $\beta$ ($\eta_0 = 1$, $G_0 = 1$, $\sigma_0 = 1$, $\gamma_0 = 0$).

## 5. POWER-LAW HEREDITARINESS OF FRACTAL MODELS OF BONES

The mechanical picture of power-law hereditariness of FHM that we reported in previous Sections does not correspond to the material organization of bone.

In this Section the authors will provide a fractal geometrical model of material specimen that corresponds to a power-law creep/relaxation function. A relation among the fractal geometric dimension of the material specimen and the exponent of the power-law is obtained. Details about fractal geometry and fractal dimension has been reported in Appendix B.

To this aim let us consider a material specimen of length measure $L_0$ and squared cross section of side length $b_0$ at the macroscopic observation scale. Let us assume, moreover, that material specimen involves several, self-similar, scale-dependent microstructures that appear with the refinement of the observation scale. Each microstructure is constituted by a bundle of longitudinal fibers of length $L_j = L_0/\varepsilon_j$, with $\varepsilon_j$ the resolution factor, $j = 1, 2, ....$ the resolution level, and $\Delta\varepsilon$ the resolution interval. Let us assume that the the cross-sectional area measure of the self-similar microstructure is scale-invariant and that it presents more and more details with the refinement of the observation scale. As a consequence, more and more detailed cross-section is present for the microstrucure observed for the $\varepsilon_{j+1}$ resolution with respect to the microstructure appearing at the $\varepsilon_j$ scale.

The requirement of self-similarity, scale-invariance measure in conjunction with the presence of more details of the microstructured cross-section yields that it must belong to a more general class of geometrical sets with respect to the Euclidean objects. An example of such class are the lacunar-type fractal sets. In Figure 9 we reported the geometrical architecture of a Sierpinski carpet, a specific precursor of fractals of side $b_0$. According to the definition of fractal dimension and fractal measure, the Sierpinski carpet has measure equal to $b_0^d/\Gamma(d-1)$, with $1 \leq d = \frac{\log(8)}{\log(3)} \leq 2$ which denotes the anomalous Hausdorff dimension. The case $d = 2$ corresponds to the well-known Euclidean set with measure $b_0^2$. As we increase the observation scale of a fractal $\varepsilon_j = j\Delta\varepsilon$, where $j = 1, 2, \ldots$ and $\Delta\varepsilon$ is the resolution interval, the fractal cross-section shows a smaller self-similar geometrical architecture still maintaining the same overall measure of the fractal cross-section area $b_0^d/\Gamma(d-1)$.



DOI: 10.1002/cnm

In this context, as we refine the resolution scale of a factor $\varepsilon_j$ to observe the $j^{th}$ microstructure, we identify geometric elements with measure $(b/\varepsilon_j)^d = b_0^d \varepsilon_j^{-d}/\Gamma(d-1)$.

We assume that the microstructure fibers are composed by a two-phase material: *i*) a purely elastic, Hookean solid phase with Young modulus $E_0$ and; *ii*) a purely viscous, Newtonian fluid phase with viscosity coefficient $\eta_0$. Let us assume that the dense space around singular points of the fractal support is occupied by the viscous phase, whereas the pores of the cross-sections are filled by the elastic phase. Since the cross-section of the material specimen possesses anomalous dimension, a scale-dependent damping coefficient $c_j$ and stiffness of the $j^{th}$ microstructure, is involved. Indeed, as we refine the observation scale of factor $\varepsilon_j$ and we measure the cross-section area at this new resolution, we must rescale the length measure of a factor $\varepsilon_j^{-d}$ to maintain the same overall measure. This geometrical consideration yields that the scaling law of stiffness and dampig coefficients of the material read (see [15] for details):

$$c_j = \frac{\eta_d b_0^d \varepsilon_j^{-d}}{L_j \Gamma(d-1)} = \frac{\eta_0}{L_0} \frac{b_0^d \varepsilon_j^{1-d}}{\Gamma(1-d)} \tag{31a}$$

$$k_j = \frac{E_d}{L_0} b_0^d \frac{\varepsilon_j^{1-d}}{\Gamma(d)} = \frac{E_0}{L_0} \frac{b_0^d \varepsilon_j^{1-d}}{\Gamma(1-d)} \tag{31b}$$

where $\eta_d = \eta_0 b^{2-d}\Gamma(d-1)/\Gamma(1-d)$ and $E_d = E_0 b^{2-d}\Gamma(d-1)/\Gamma(1-d)$is the anomalous viscosity coefficient.

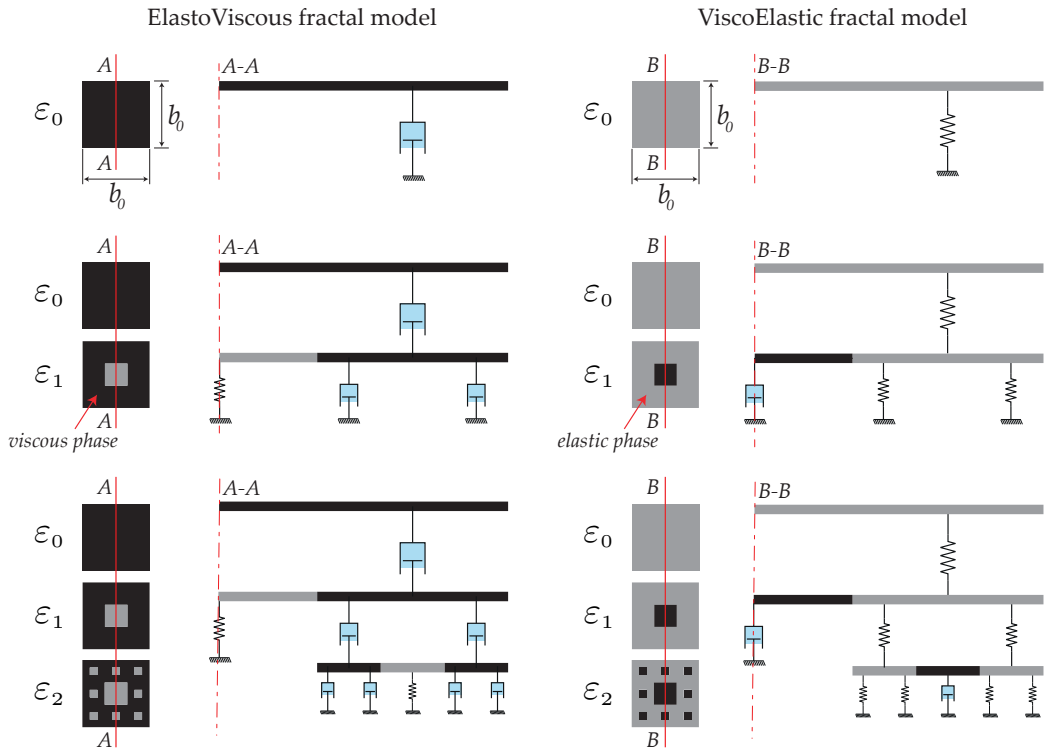


Figure 9. Fractal mechanical representation of the elastic and viscous phase of the material microstructure.

The presence of a material microstructure that is maintained, as we refine the observation scale, togheter with a new microstructure appearing at smaller scales involves a connection among the different microstructures as observed by the mechanical fractance in Figure 9. To this aim we reported in Figure 9 the micromechanical fractal tree corresponding to section A-A of the Sierpinsky carpet modelling the EV and VE Material, respectively. The elastic (for VE material), as well as the viscous (for EV material), phase are distributed among scales in a self-similar fashion, filling pores with an Hookean or Newtonian material, respectively.



DOI: 10.1002/cnm

It must be remarked that, as we consider the presence of self-similar microstructures appearing at different observation scales, still maintaining previously observed microstructures, is not corresponding to the classical mechanical discussions on fractal sets. Indeed the introduced material model is not equivalent to the analysis of a fractal-like solid that involves, instead different microstructures at different scales without any interaction among the scales.

The kinematic degrees of freedom of the microstructure observed at different scales are defined as $u_j$ and, in this regard, the mechanical fractance is fully equivalent to a mechanical hierarchical assembly of viscous dashpots with damping coefficients $c_j$ externally restrained by linear springs with stiffness coefficients $k_j$ as reported in Figure 10:

The balance of linear momentum involves contributions from the $j-1$ and $j+1$ observation scales and, the system of differential equation ruling the time-evolution of the microstructure displacements may be written as:

$$\begin{aligned}
&F = c_1\left(\dot{u}_1 - \dot{u}_2\right) + k_1 u_1 \\
&c_1\frac{\left(\dot{u}_1 - \dot{u}_2\right)}{\Delta\varepsilon} = c_2\frac{\left(\dot{u}_2 - \dot{u}_3\right)}{\Delta\varepsilon} + k_2 u_2 \Delta\varepsilon \\
&c_2\frac{\left(\dot{u}_2 - \dot{u}_3\right)}{\Delta\varepsilon} = c_3\frac{\left(\dot{u}_3 - \dot{u}_4\right)}{\Delta\varepsilon} + k_3 u_3 \Delta\varepsilon \\
&\vdots \\
&c_{j-1}\frac{\left(\dot{u}_{j-1} - \dot{u}_j\right)}{\Delta\varepsilon} = c_j\frac{\left(\dot{u}_j - \dot{u}_{j+1}\right)}{\Delta\varepsilon} + k_j u_j \Delta\varepsilon \\
&\vdots
\end{aligned} \tag{32}$$

The use of the Laplace transform allows for solving the system reported in (32) in the following

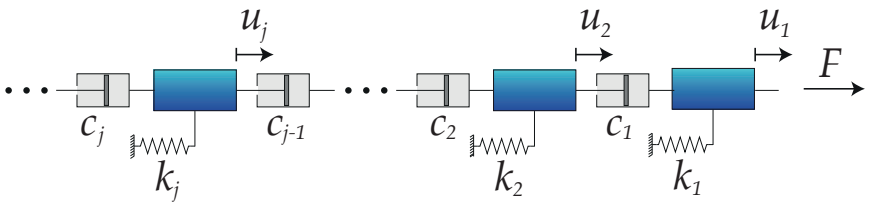


Figure 10. The mechanical hierarchy of the microstructure at the $j^{\text{th}}$ observation scale.

form:

$$\tilde{u}_1(s) = \frac{\tilde{F}(s)}{k_1}\frac{1}{f_1} - \frac{\tilde{\tau}_1\tilde{\tau}_2}{f_2} - \frac{\tilde{\tau}_2\tilde{\tau}_3}{f_3} - \cdots \frac{\tilde{\tau}_{j-1}\,\tilde{\tau}_j}{f_j} - \cdots \tag{33}$$

where the symbol denoting the continued fractions was used (see Appendix C for more details). In (33) we defined the quantities $\tilde{\tau}_j = s\,\bar{c}_j/\bar{k}_j$, $f_j = 1 + r_j + \tilde{\tau}_j$ and $r_j = s\,\bar{c}_{j-1}/\bar{k}_j$ in order to get a compact form of the expression, where $\bar{k}_j = k_j\Delta\varepsilon$ and $\bar{c}_j = c_j/\Delta\varepsilon$. Moreover, the quantity $\tilde{\tau}_j$ represent the relaxation time at the $j^{\text{th}}$ observation scale. The substitution in (32) of the stiffness $k_j$ and the viscosity $c_j$ using (14a) and (14b), respectively, and replacing $\Delta z$ with $\Delta\varepsilon$ yields the following differential equation as $\Delta\varepsilon \to 0$:

$$\frac{E_0}{\Gamma(1-d)}\varepsilon^{1-d}u(\varepsilon,t) = \frac{\partial}{\partial\varepsilon}\left[\frac{\eta_0}{\Gamma(1-d)}\varepsilon^{1-d}\frac{\partial\dot{u}(\varepsilon,t)}{\partial\varepsilon}\right] \tag{34}$$

with boundary conditions stated as:

$$u(\infty,t) = 0 \tag{35a}$$

$$F = \lim_{\varepsilon\to 0}\frac{\eta_0}{\Gamma(1-d)}b^d\frac{\partial\dot{u}}{\partial\varepsilon}\varepsilon^{1-d}, \tag{35b}$$



DOI: 10.1002/cnm

(see Sect. IV in [15] for an analog derivation). The observation of (34,35) shows that assuming $\alpha = d - 1$, the solution for $\varepsilon \to 0$ yields a displacement-force rheological relation as:

$$F_0 = C_\beta \left( \mathrm{D}^{\beta}_{0^+} u \right)(t) \tag{36}$$

with a relation among the decaying coefficient $\beta$, the proportionality coefficient $C_\beta$ and the fractal dimension of the cross-section area that reads:

$$\beta = \frac{(1-\alpha)}{2} = \frac{(2-d)}{2}, \qquad C_\beta = \frac{G_0 \Gamma(\frac{2-d}{2})}{\Gamma(d)\Gamma(d/2) 2^{d-1}} \left(\tau_E(\alpha)\right)^{\frac{(2-d)}{2}} \tag{37}$$

with $\tau_E(\alpha) = -\frac{\eta_0}{G_0} \frac{\Gamma(d-1)}{\Gamma(1-d)}$. We observe that, as $d = 2$, the Euclidean dimension of the cross-section yields a perfectly elastic material. In case $d = 1$, instead a fractional hereditary material at critical state, that is with exponent $\beta = 1/2$, is obtained.

The case involving VE material, i.e. with $1/2 \leq \beta \leq 1$ may be dealt with similar arguments yielding a relation among the power-law exponent and the fractal dimension as $\beta = d/2$. More details about the fractal representation of material hereditariness will be reported in a forthcoming paper [43].

Summing up, we observed that, introducing a fractal geometric description of the microstructure of material specimen, a relation among the power-law exponent of creep/relaxation function and the fractal dimension of the geometric cross-section may be obtained.

As the relation among Hausdorff dimension and power-law exponent has been established the application may be devoted to a fractal model of the bone tissue hereditariness. Indeed in Figure 11 c we reported the Hausdorff dimension of a rat femural cross-section trabecular structure at resolution scales ($cm - \mu m$).

The fractal dimension have been obtained, by an isthological specimen of bone tissue of a bone head after a period in fornaline for 24 hours. Bone specimen have been then decalcified in EDTA with an acid tampon and, furthermore reconditioning have been performed with Phosphate Buffered Saline (PBS). The specimen have been also immersed in alchoolical solutions with different concentrations,left in xilene solution, and immersed in paraffine at 60 °C for two hours.

The observation of the prepared bone tissue specimen have been performed on an optical microscope after coloration of the bone marrow with emathossiline-eosin and observed in the range from 10x to 40x with a Leica DM 5000 B with camera CCD Leica 3000 F as in Figure 11a. The observed images have been then recomposed to cover the entire rat femoural head and the evaluation of the fractal dimension of the bone head has been performed on a binary image conversion as in Figure 11b). The fractal dimension have been obtained by means of the box-counting method (see Appendix B for more details) obtaining, for the different specimen analized, fractal dimension in the range $\Delta_r = 1.70 - 1.83$. A representation of the fractal dimension has been reported in the Log-Log representation in Figure 11c

With the estimated values of Hausdorff dimension $\Delta_r$ we may conclude that the cross-sectional area of a bone head is not Euclidean and, by recalling previous arguments, a relation among the fractal dimension and the creep/relaxation exponent may be provided (with $\Delta_r = 1.83$) as $\beta = (2-d)/2 = (2-\Delta_r)/2 = 0.085$. This value is very close to the estimated one for $\beta$, obtained from macroscopic mechanical experimental tests as reported in Section 2 on different bone tissues specimens.

However, it may be observed that the bone tissue has a hierarchical self-organization and that, at different resolution scales, different geometric structures may be observed [8]. Indeed, bones are not true fractal since they do not posses a self-similar organization at every resolution scale and, therefore, a fractal model of bone tissue may be only a rough approximation.

In this regard, we observe that the lack of self-similarity of real bone is limited to the difference among observed hierarchic levels of bone tissue (see Figure 12).

However, for each element of the hierarchy a specific value of the fractal dimension $\Delta_k$, with $k = 1, 2, \ldots, N$ ($N$ represents the number of level of the hierarchy), may be identified. As we observe that for each level of the hierarchy an elastic and a viscous phase exists and more details in



DOI: 10.1002/cnm

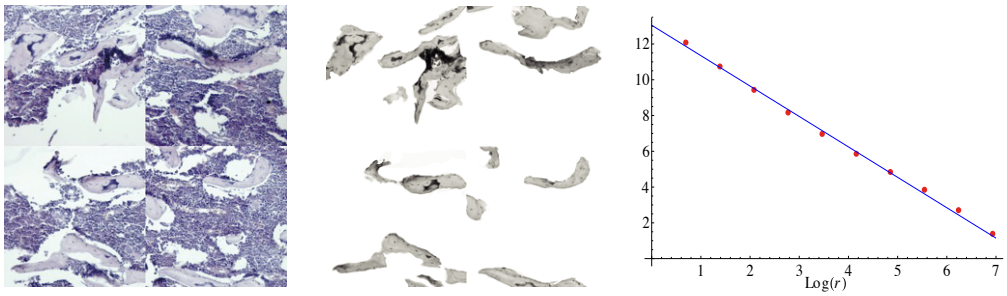


Figure 11. (a) High resolution image of a cross-section of a health rat bone proximis femural epiphisis after chemical treatment (as deffatting). (b) Image elaboration oriented to highlight the resistant section. (c) Evaluation of the fractal dimension using the box-counting method (see Appendix B for more details).

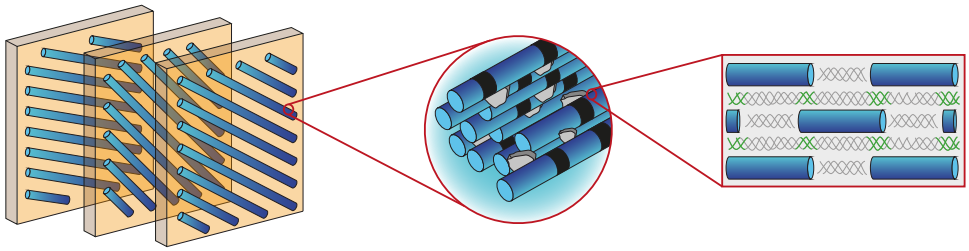


Figure 12. (a) Bone Lamellae scale. (b) Collagen fibers scale. (c) Collagen fibrils scale.

their separation may be obtained increasing the resolution scale, within the range of the observed hierarchical structure a relation as $\beta_k = (2 - \Delta_k)/2$ may be provided. In this case a model involving linear combinations of power-laws with $C_{\beta_1} t^{\beta_1} + C_{\beta_2} t^{\beta_2} + \dots$ may be build providing a better estimate of creep and relaxation functions. Details about this possibility to model material behavior will be reported elsewhere.

We conclude this Section observing that the FHM model with a single power-law with exponent $\overline{\beta}$ may represent the creep/relaxation of a multiple hierarchic fractal geometry with averaged dimension $\overline{\Delta} = \left(\sum_{k=1}^{N} p_k \Delta_k\right)/N$ with $0 \leq \beta_k \leq 1$ and $p_k$, $k = 1, 2, ..., N$ weighting coefficients $0 \leq p_k \leq 1$ useful to provide the influences of the $j^{\text{th}}$ scale to the overall hereditariness of material specimen. In this latter case the value of the exponent of the power-law creep/relaxation may be obtained as $\overline{\beta} = (2 - \overline{d})/2$.

## 6. CONCLUSIONS

Mineralized biological tissues, like bones, tendons and ligaments, must provide carrying-load capacity in mammalian organism. In this regard the mechanical behavior of these tissues as of other highly functionalized tissues are very important in biomedical engineering. Indeed, the main feature that biomedical devices must possess have high compatibility with directly interacting biological tissues. For natural and artificial bone-like structures, this feature involves similar stiffness, strength and toughness among in vivo and artificial devices. The bones can grow, change their form during their life and self-heal after a fracture, renewing through a remodeling process. All these processes are regulated by mechanical, hormonal and physiological signals. In particular osteocytes basic remodelling is mainly led by mechanical transduction through strain/energy density in bone tissue



DOI: 10.1002/cnm

[19, 44, 45, 46, 47] and, henceforth, the hereditariness of mineralized biological tissue is a crucial aspect to detect the speed of bone reformations as well as to predict its interactions with artificial devices.

In this study the authors aimed to face this problem in the advanced framework of fractal geometry and fractional-order calculus . Indeed, macroscopic hereditariness of bone tissue is well fit by power-law relaxation and creep functions, yielding stress and strain constitutive behavior in terms of the so-called fractional order integral and derivatives. It is shown that the power-law functions experienced in mechanical tests at macroscale may be captured by a fractal scaling of the microstructure cross-section. Indeed it has been shown that material specimen involving a self-similar microstructure at any observation scale with anomalous scaling is strictly related with a mechanical hierarchic model. As the presence of two-phases, a purely viscous one and a purely elastic one is involved, then a relation among the fractional-differentiation order and the anomalous geometrical scaling of the cross-section is obtained. Some experimental tests on a rat femoral head from macro-to-micro scales has shown that bone cross-section possesses anomalous scaling and a model of fractal-type bone microstructure may be introduced. The relation among the fractional-order derivation index and the fractal dimension of bone model has been established and, by means of the measured value of the fractal dimension, the fractional-order index obtained is very close to its estimates from mechanical tests. Proper details and generalizations will be reported in forthcoming papers [43].

ACKNOWLEDGEMENTS

Luca Deseri acknowledges the Center for Nonlinear Analysis through the NSF Grant No. DMS-0635983 and University of Trento through the Grant "Computational Mechanics 2013". M. Di Paola and M. Zingales are very grateful to research Grant No. Prin 2010-2011, National Coordinator Professor A. Luongo. Pietro Pollaci acknowledges the Doctoral School in Engineering of Civil and Mechanical Structural Systems, University of Trento for the financial support.

## APPENDIX A. FUNDAMENTAL DEFINITIONS OF FRACTIONAL ORDER CALCULUS

Fractional calculus may be considered the extension of the ordinary differential calculus to non-integer powers of derivation orders (e.g. see [13, 14]). In this Appendix we address some basic notions about this mathematical tool.

The Euler-Gamma function $\Gamma(z)$ may be considered as the generalization of the factorial function since, as $z$ assumes integer values as $\Gamma(z+1) = z!$ and it is defined as the result of the integral as follows:

$$\Gamma(z) = \int_0^\infty e^{-x} x^{z-1} dx. \tag{A1}$$

The Riemann-Liouville fractional integrals and derivatives with $0 < \beta < 1$ of functions defined on the entire real axis $\mathbb{R}$ have the following forms:

$$\left(\mathrm{I}_+^\beta f\right)(t) = \frac{1}{\Gamma(\beta)} \int_{-\infty}^t \frac{f(\tau)}{(t-\tau)^{1-\beta}} d\tau \tag{A2a}$$

$$\left(\mathrm{D}_+^\beta f\right)(t) = \frac{1}{\Gamma(1-\beta)} \frac{d}{dt} \int_{-\infty}^t \frac{f(\tau)}{(t-\tau)^{\beta}} d\tau. \tag{A2b}$$

The Riemann-Liouville fractional integrals and derivatives with $0 < \beta < 1$ of functions defined over intervals of the real axis, namely $f(t)$ such that $t \in [a, b] \subset \mathbb{R}$, have the following forms:

$$\left(\mathrm{I}_a^\beta f\right)(t) = \frac{1}{\Gamma(\beta)} \int_a^t \frac{f(\tau)}{(t-\tau)^{1-\beta}} d\tau \tag{A3a}$$

$$\left(\mathrm{D}_a^\beta f\right)(t) = \frac{f(a)}{\Gamma(1-\beta)(t-a)^{\beta}} + \frac{1}{\Gamma(1-\beta)} \int_a^t \frac{f'(\tau)}{(t-\tau)^{\beta}} d\tau. \tag{A3b}$$



DOI: 10.1002/cnm

The relation (A3b) is a direct consequence of Corollary of Lemma 2.1 in [14] (p.32). Beside Riemann-Liouville fractional operators defined above, another class of fractional derivative that is often used in the context of fractional viscoelasticity is represented by Caputo fractional derivatives defined as:

$$\left({}_C\mathrm{D}^{\beta}_{a^+} f\right)(t) := \mathrm{I}^{m-\beta}_{a^+}\left(\mathrm{D}^{m}_{a^+} f\right)(t) \quad m-1<\beta<m \tag{A4}$$

and whenever $0<\beta<1$ it reads as follows:

$$\left({}_C\mathrm{D}^{\beta}_{a^+} f\right)(t) = \frac{1}{\Gamma(1-\beta)}\int_a^t \frac{f'(\tau)}{(t-\tau)^{\beta}}d\tau. \tag{A5}$$

A closer analysis of (A3b) and (A5) shows that Caputo fractional derivative coincides with the integral part of the Riemann-Liouville fractional derivative in bounded domain. Moreover, the definition in (A4) implies that the function $f(t)$ has to be absolutely integrable of order $m$ (e.g. in (A5) the order is $m=1$). Whenever $f(a)=0$ Caputo and Riemann-Liouville fractional derivatives coalesce.

Similar considerations hold true also for Caputo and Riemann-Liouville fractional derivatives defined on the entire real axis. Caputo fractional derivatives may be consider as the interpolation among the well-known, integer-order derivatives, operating over functions $f(\circ)$ that belong to the class of Lebesgue integrable functions ($f(\circ)\in L^1$) as a consequence, they are very useful in the mathematical description of complex system evolution.

It is worth introducing integral transforms for fractional operators. Similarly to classical calculus, the Laplace integral transform $\mathcal{L}(\circ)$ is defined in the following forms:

$$\mathcal{L}\left[\left(\mathrm{D}^{\beta}_{0^+} f\right)(t)\right] = s^{\beta}\mathcal{L}[f(t)] = s^{\beta}\tilde{f}(s) \tag{A6a}$$

$$\mathcal{L}\left[\left(\mathrm{I}^{\beta}_{0^+} f\right)(t)\right] = s^{-\beta}\mathcal{L}[f(t)] = s^{-\beta}\tilde{f}(s). \tag{A6b}$$

In the same way, the Fourier integral transform $\mathcal{F}(\circ)$ assumes the following forms:

$$\mathcal{F}\left[\left(\mathrm{D}^{\beta}_{+} f\right)(t)\right] = (-i\omega)^{\beta}\mathcal{F}[f(t)] = (-i\omega)^{\beta}\hat{f}(\omega) \tag{A7a}$$

$$\mathcal{F}\left[\left(\mathrm{I}^{\beta}_{+} f\right)(t)\right] = (-i\omega)^{-\beta}\mathcal{F}[f(t)] = (-\omega)^{-\beta}\hat{f}(\omega). \tag{A7b}$$

We recall that the Laplace and Fourier integral transforms are defined as follows:

$$\mathcal{L}[f(t)] = \int_0^{\infty} f(t)\mathrm{e}^{-st}dt \tag{A8a}$$

$$\mathcal{F}[f(t)] = \int_{-\infty}^{+\infty} f(t)\mathrm{e}^{-i\omega t}dt. \tag{A8b}$$

These mathematical tools may be very useful to solve systems of fractional differential equations, which *appear more and more frequently in various research areas and engineering applications* [13]. The research on electrical circuits (especially on semiintegrating circuits) was one of the first fields of application of differential equations of fractional order [91]. As example we consider the following differential equation of order $\beta=1/2$:

$$\left(\mathrm{D}^{\frac{1}{2}}_{0} f\right)(t) + af(t) = 0 \tag{A9}$$

with the following initial condition

$$C = \left[\left(\mathrm{D}^{-\frac{1}{2}}_{0} f\right)(t)\right]_{t=0}. \tag{A10}$$

The use of the Laplace integral transform allows for writing the solution in the Laplace domain as follows:

$$\tilde{f}(s) = \frac{C}{s^{1/2}+a}. \tag{A11}$$

Whenever the time domain is restored, the solution has the following form:

$$f(t) = Ct^{-\frac{1}{2}}E_{\frac{1}{2},\frac{1}{2}}\left(-a\sqrt{t}\right) \tag{A12}$$



DOI: 10.1002/cnm

where $E_{\alpha,\beta}(z)$ is the Mittag-Leffler function, defined as follows:

$$E_{\alpha,\beta}(z) = \sum_{k=0}^{\infty} \frac{z^k}{\Gamma(\alpha k + \beta)} \qquad \alpha > 0\ ,\ \beta > 0. \tag{A13}$$

In the textbook of Podlubny [13] (p. 21) an expression for the Laplace transform can be found in the following form

$$\mathcal{L}\left[t^{\frac{k-1}{2}} E^{(k)}_{\frac{1}{2},\frac{1}{2}}\left(a \pm \sqrt{t}\right)\right] = \frac{k!}{\left(\sqrt{s} \mp a\right)^{k+1}} \tag{A14}$$

where the notation $^{(k)}$ denotes the $k^{th}$-derivative. We recognize that in (A11) $k = 0$, henceforth the time domain solution reads has the form reported in (A12).

The curious reader can find several procedures and examples on differential equations of fractional order in the complete textbooks by Podlubny [13] and Samko [14].

## APPENDIX B. FUNDAMENTALS OF FRACTAL GEOMETRY

The *fractal geometry* (from the Latin word *fractus*, extremely divided) was introduced by Mandelbrot [92] at the end of the seventies in order to give scholars a new mathematical tool to describe *real* objects. The notions stated by Mandelbrot have spread in several field of research, such as chaos and financial theories [93, 94]

The particular property of the fractal objects is the self-similarity. This property means, roughly speaking, that the object may be defined as the union of smaller, self-similar copies of itself. Such a property of fractal objects may also be used to define fractals by means of self-similar transformations of the parent object. This feature has to be understood rigorously for mathematical fractals only, whereas it has to be interpreted in a statistical sense for real objects.

The measure of fractal objects as well as their dimension are the main differences with respect to their Euclidean description. The classical Euclidean objects are characterized by *integer* dimension which identifies the degrees of freedom of the object in the related Euclidean space. On the contrary, the dimension of the fractal objects is different from one of the Euclidean space which encloses them; whenever the dimension of the fractal object is greater than the one of the Euclidean space it is defined *lacunar*, otherwise it is *invasive*.

Several authors [95] tried to provide a mathematical definition of fractal dimensions. The most used definitions have been addressed by Mandelbrot [92], Hausdorff and Besikovitch [96] and Minkowski [97]. The first is related to the invariance property under change of observation scale of fractal objects, whereas the latter ones depend on the coverage density of fractal object by Euclidean covers.

The Mandelbrot's dimension $\Delta$ is strictly related to the Mandelbrot's fundamental relation as follows:

$$N r^{\Delta} = L_0^{\Delta} \quad \Longrightarrow \quad \Delta = \frac{\log N}{\log \frac{L_0}{r}} \tag{B1}$$

where $N$ is the number of self-similar copies when the observation scale changes, $L_0$ is the length of the parent object and $r$ is the length of the ruler.

In order to define the Hausdorff-Besikovitch dimension, it is worth to introduce the concept of Hausdorff-measure. Let $U$ be a non-empty set enclosed in $\mathbb{R}^n$. The diameter of this set is defined as the greater distance between two any points belonging to it, i.e. $|U| = \sup\{|x - y| : x, y \in U\}$. The $\delta$-cover of a fractal subset $F$ depends on the parameter $\delta$ as follows:

$$F \subset \bigcup_{i=1}^{\infty} U_i \quad |U|_i \leq \delta \tag{B2}$$

where $\delta$ represents the greater diameter allowed. Let $\alpha$ be a non-negative real number. For all $\delta \geq 0$, the Hausdorff measure is defined in the following form:

$$\mathcal{H}^{\alpha}_{\delta} = \lim_{\delta \to 0} \inf \left\{ \sum_{i=1}^{\infty} |U|_i^{\alpha} : |U|_i \text{ is a } \delta\text{-cover of } F \right\}. \tag{B3}$$

The value of the limit defined in (B3) is either 0 or $\infty$, except for a specific choice of $\overline{\alpha}$ in correspondence to which the curve $\mathcal{H}^{\alpha}(F)$ have a jump (see Figure 13). The Hausdorff-Besikovitch dimension $d_H$ of a fractal object $F$ is defined as the smaller value of $\alpha$ such that the Hausdorff measure of $F$ has zero value or,



DOI: 10.1002/cnm

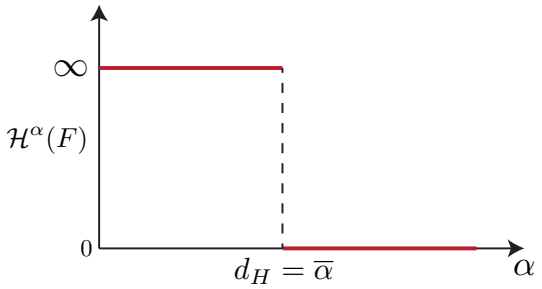


Figure 13. The Hausdroff-Besikovitch dimension of a fractal object $\mathcal{H}^{\alpha}(F)$.

equivalently, the greater value of $\alpha$ such that the Hausdorff measure of $F$ has infinite value :

$$d_H(F) = \overline{\alpha} = \sup\{\alpha : \mathcal{H}^{\alpha}(F) = \infty\} = \inf\{\alpha : \mathcal{H}^{\alpha}(F) = 0\}. \tag{B4}$$

The Hausdorff dimension is an integer number for the Euclidean objects whereas it is a real number for the fractal ones.

The last definition of dimension was proposed by Minkowski [97] and after studied by Bouligand [98] and Kolomogorov [99]. The observer selects a proper coverage box (e.g. a range, a square and a cube for 1D, 2D and 3D Euclidean spaces respectively) and computes how many objects need to completely cover the fractal object when the amplitude of the cover decreases. The computation of the slow of the best fitting straight-line in the bi-logarithmic plane allows for calculating the fractal dimension as follows:

$$d_{MB} = \lim_{\delta \to 0} \left[ D - \frac{\log F(\delta)}{\log \delta} \right] \tag{B5}$$

where $D$ is the dimension of the Euclidean space in which the object is enclosed, $\delta$ is the dimension of the cover and $F(\delta)$ is the overall coverage (union of all covers of the object). This procedure is the most used since it is easily enforced in numerical codes.

## APPENDIX C. FUNDAMENTALS OF CONTINUED FRACTION

The continued fractions give an exact mathematical representation of rational and irrational numbers. For instance, the exact representation of 67/29 reads as:

$$\frac{67}{29} = 2 + \frac{1}{3 + \frac{2}{9}}. \tag{C1}$$

The use of this powerful mathematical tool is strictly related to need to find a better mathematical representation of the decimal one. The *general* definition of continued fraction can be expressed in the following form:

$$f = b_0 + \cfrac{a_1}{b_1 + \cfrac{a_2}{b_2 + \cfrac{a_3}{b_3 + \ddots}}} \tag{C2}$$

where $a_n$ and $b_n$, namely the *elements* of the continued fraction, are complex numbers and $a_m \neq 0$ for all $m$. The numbers $a_m$ and $b_m$ are called $m^{\text{th}}$ *partial numerator* and *partial denominator*. Whenever $a_m = 1$ for all m, equation (C2) is defined *simple* continued fraction. A more convenient form for (C2) can be written as follows:

$$f = b_0 + \frac{a_1}{b_1} + \frac{a_2}{b_2} + \frac{a_3}{b_3} + \ldots. \tag{C3}$$

Let $\{a_m\}_{m \in \mathbb{N}}$ and $\{b_m\}_{m \in \mathbb{N}}$ an ordered pair of complex numbers, where $\mathbb{N}_0$ and $\mathbb{N}$ are the set of the positive integer including or not the 0 respectively. It is possible to define a linear fractional transformation as follows:

$$s_0(w) := b_0 + w \qquad s_n(w) := \frac{a_n}{b_n + w} \qquad n = 1, 2, 3, \ldots \tag{C4}$$

$$S_0(w) := s_0(w) \qquad S_n(w) := S_{n-1}\left(s_n(w)\right) \qquad n = 1, 2, 3, \ldots \tag{C5}$$



DOI: 10.1002/cnm

The form assumed by (C5) for a generic value of $w$ is the following:

$$S_n(w) = b_0 + \cfrac{a_1}{b_1 + \cfrac{a_2}{b_2 + \cfrac{a_3}{b_3 + \ddots \cfrac{a_n}{b_n + w}}}} \tag{C6}$$

Whenever the number $f$ is rational the elements of the continued fraction coalesce with the Euclidean algorithm and they are finite; otherwise if $f$ is irrational the continued fraction is composed by an infinite number of elements. The $n^{\text{th}}$ approximation of an irrational number can be written as follows:

$$f_n = b_0 + \frac{a_1}{b_1} + \frac{a_2}{b_2} + \frac{a_3}{b_3} + \cdots + \frac{a_n}{b_n}. \tag{C7}$$

Every rational number has an essentially unique continued fraction representation.

The continued fraction have been used to give more accurate description of several mathematical functions (such as exponential, power-law, trigonometric, hyperbolic, error, Bessel functions and many other) and constants (Euler's number, Euler's constant, golden ratio and many other) and also in the eigen-analysis. The curious reader can find more details are deeply treated in the complete *Handbook of Continued Fractions for Special Function* [100].

## References


1. Metzler R, Klafter J. The random walk's guide to anomalous diffusion: A fractional dynamics approach. *Physics Reports* 2000; **399**:1–77.
2. Ammann P, Rizzoli R. Bone strength and its determinants. *Osteoporosis International* 2003; **14**:S13–S18.
3. Seeman E, Delmas PD. Bone quality — the material and structural basis of bone strength and fragility. *The New England Journal of Medicine* 2006; **354**:2250–2261.
4. Gao H. Application of fracture mechanics concepts to hierarchical biomechanics of bone and bone-like materials. *International Journal of Fracture* 2006; **138**:101–137.
5. Hellmich C, Barthélémy JF, Dormieux L. Mineral-collagen interactions in elasticity of bone ultrastructure - a continuum micromechanics approach. *European Journal of Mechanics A/Solids* 2004; **23**:783–810.
6. Katti DR, Pradhan SM, Katti KS. Directional dependence of hydroxyapatite-collagen interactions on mechanics of collagen. *Journal of Biomechanics* 2010; **43**:1723–1730.
7. Bhowmik R, Katti KS, Verma D, Katti DR. Probing molecular interactions in bone biomaterials: Through molecular dynamics and fourier transform infrared spectroscopy. *Materials Science and Engineering C* 2007; **27**:352–371.
8. Lakes R. Materials with structural hierarchy. *Nature* 1993; **361**:511–515.
9. Nikolov S, Raabe D. Hierarchical modeling of the elastic properties of bone at submicron scales: The role of extrafibrillar mineralization. *Biophysical Journal* 2008; **94**:4220–4232.
10. Muller R. Hierarchical microimaging of bone structure and function. *Nature Reviews* 2009; **5**:373–381.
11. Iyo T, Maki Y, Sasaki N, Nakata M. Anisotropic viscoelastic properties of cortical bone. *Journal of Biomechanics* 2004; **37**:1433–1437.
12. Mainardi F. *Fractional Calculus and Waves in Linear Viscoelasticity*. Imperial College Press, 2010.
13. Podlubny I. *Fractional Differential Equation*. Academic, New York, 1998.
14. Samko SG, Kilbas AA, Marichev OI. *Fractional Integrals and Derivatives. Theory and Applications*. Gordon & Breach Science Publishers: Londn - New York, 1987.
15. Di Paola M, Zingales M. Exact mechanical models of fractional hereditary materials. *Journal of Rheology* 2012; **56**(5):983–1004.
16. Hellmich C, Ulm FJ. Drained and undrained poroelastic properties of healthy and pathological bone: a poro-micromechanical investigation. *Transport in Porous Media* 2005; **58**:243–268.
17. Hellmich C, Ulm F. Microporodynamics of bones: Prediction of the "frenkel-biot" slow compressional wave. *Journal of Engineering Mechanics* September 2005; **131**(9):918–927.
18. Hellmich C, Celundov D, Ulm FJ. Multiporoelasticity of hierarchically structured materials: micromechanical foundations and application to bone. *Journal of Engineering Mechanics* 2009; **135**(5):382–394.
19. Pivonka P, Zimak J, Smith DW, Gardiner BS, Dunstan CR, Sims NA, Martin TJ, Mundy GR. Model structure and control of bone remodeling: A theoretical study. *Bone* 2008; **43**:249–263.
20. Cowin SC. Bone poroelasticity. *Journal of Biomechanics* 1999; **32**:217–238.
21. Deseri L, Owen DR. Toward a field theory for elastic bodies undergoing disarrangements. *Journal of Elasticity* 2003; **70**(I):197–236.
22. Deseri L, Owen DR. Submacroscopically stable equilibria of elastic bodies undergoing disarrangements and dissipation. *Mathematics and Mechanics of Solids* 2010; **15**(6):611–638.
23. Deseri L, Owen DR. Moving interfaces that separate loose and compact phases of elastic aggregates: a mechanism for drastic reduction or increase in macroscopic deformation. *Continuum Mechanics and Thermodynamics* 2012; doi:10.1007/s00161-012-0260-y.
24. Werner HJ, Martin H, Behrend D, Schmitz KP, Schoherf HC. The loss of stiffness as osteoporosis progresses. *Medical Engineering & Physics* 1996; **18**(7):601–606.

25. McDonald K, Little J, Pearcy M, Adam C. Development of a multi-scale finite element model of the osteoporotic lumbar vertebral body for the investigation of apparent level vertebra mechanics and micro-level trabecular mechanics. *Medical Engineering & Physics* 2010; **32**:653–661.
26. Stein MS, Thomas SA C D L amd Feik, Wark JD, Clement JG. Bone size and mechanics at the femoral diaphysis across age and sex. *Journal of Biomechanics* 1998; **31**:1101–1110.
27. Quaglini V, La Russa V, Corneo S. Nonlinear stress relaxation of trabecular bone. *Mechanics Research Communications* 2009; **36**:275–283.
28. Abdel-Wahab A, Alam K, Silberschmidt V. Analysis of anisotropic viscoelastoplastic properties of cortical bone tissues. *Journal of The Mechanical Behavior of Biomedical Materials* 2011; **4**:807–820.
29. Wang Y, Zhang Z, Hei F, Ma H. Experimental study on the viscoelastic properties of cancellous bone of the os calcaneus, os lunatum and os capitalum]. *Journal of Biomedical Engineering* Sept 2003; **20**(3):434–438.
30. Poundarik AA, Diab T, Sroga GE, Ural A, Boske A, Gundberg CM, Vashishth D. Dilatational band formation in bone. *PNAS Early Edition* 2012; .
31. Cowin SC, Doty SB. *Tissue Mechanics*. Springer, 2007.
32. Gautieri A, Vesentini A, Redaelli A, , Buehler MJ. Hierarchical structure and nanomechanics of collagen microfibrils from the atomistic scale up. *American Chemical Society Nano Letters* 2011; **11**:757–766 757–766 757–766.
33. Morgan EF, Bayraktar HH, Keaveny TM. Trabecular bone modulus–density relationships depend on anatomic site. *Journal of Biomechanics* 2003; **36**:897–904.
34. Deseri L, Zingales M, Pollaci P. On the notion of state of fractional hereditary materials (fhm). *Submitted* ; .
35. Del Piero G, Deseri L. On the concepts of state and free energy in linear viscoelasticity. *Archive for Rational Mechanics and Analysis* 1998; **138**:1–35.
36. Deseri L, Golden MJ, Fabrizio M. The concept of a minimal state in viscoelasticity: New free energies and applications to pdes. *Archive for Rational Mechanics and Analysis* 2006; **181**:43–96.
37. Friedrich C. Relaxation and retardation functions of the maxwell model with fractional derivatives. *Rheologica Acta* 1991; **30**(2):151–158.
38. Friedrich C. Mechanical stress relaxation in polymers: Fractional integral model versus fractional differential model. *Non-Newtonian Fluid Mechanics* 1993; **46**:307–314.
39. Friedrich C, Braun H. Linear viscoelastic behaviour of complex polymeric materials: A fractional mode representation. *Colloid & Polymer Science* 1994; **272**:1536–1546.
40. Scott Blair G. The role of psychophysics in rheology. *Journal of Colloid Science* 1947; **2**:21–32.
41. Di Paola M, Pinnola F, Zingales M. Fractional differential equations and related exact mechanical models. *(Submitted)* 2012; .
42. Di Paola M, Pinnola FP, Zingales M. A discrete mechanical model of fractional hereditary materials. *Meccanica* 2013; .
43. Di Paola M, Zingales M. Fractal bodies hereditariness: The power-laws. *Journal of Rheology* submitted; .
44. Burger EH. Experiments on cell mechanosensivity: bone cells as mechanical engineers. *Bone Mechanics Handbook* 2001; .
45. Cowin SC, Moss-Salentijn L, e Moss ML. Candidates for the me- chanosensory system in bone. *Journal of Biomechanical Engineering* 1992; **113**(2).
46. Thomsen JS, Mosekilde L, Boyce RW, Mosekilde E. Stochastic simulation of vertebral trabecular bone remodeling. *Bone* 1994; **15**(6):655–666.
47. Martin TJ, Seeman E. Bone remodelling: its local regulation and the emergence of bone fragility. *Best Practice & Research Clinical Endocrinology & Metabolism* 2008; **22**(5):701–722.
48. Gao H. Modeling fracture in nano materials via a virtual internal bond method. *Engineering Fracture Mechanics* 2003; **70**:1777–1791.
49. Gao H, Ji B, Jager I, Arzt E, Fratzl P. Materials become insensitive to flaws at nanoscale: Lessons from nature. *Applied Physical Science* 2003; **100**:5597–5600.
50. Ji B, Gao H. Mechanical properties of nanostructure of biological materials. *Journal of Mechanics and Physics of Solids* 2004; **52**:1963–1990.
51. Ji B, Gao H. A study of fracture mechanisms in biological nano-composites via the virtual internal bondmodel. *Materials Science and Engineering A* 2004; **366**:96–103.
52. Gao H, Yao H. Shape insensitive optimal adhesion of nanoscale fibrillar structures. *Applied Physical Science* 2004; **101**(21):7851–7856.
53. Gao H, Wang X, Yao H, Gorb S, Arzt E. Mechanical principles of a self-similar hierarchical structure. *Mechanics of Materials* 2005; **37**:275–285.
54. Yao H, Gao H. Multi-scale cohesive laws in hierarchical materials. *International Journal of Solids and Structures* 2007; **44**:8177–8193.
55. Fratzl P, Groschner M, Vogl G, Plenk Jr H, Eschberger J, Fratzl-Zelman F, Koller K, Dr Klaushofer K. Mineral crystals in calcified tissues: A comparative study by saxs. *Journal of Bone and Mineral Research* 1992; **7**:329–334.
56. Fratzl P. Cellulose and collagen: from fibres to tissues. *Current Opionion in Colloid and Interface Science* 2003; **8**:32–39.
57. Ascenzi A, Bonucci E. The tensile properties of single osteons. *The Anatomical Record* 1967; **158**:375–386.
58. Ascenzi A, Bonucci E. The compressive properties of single osteons. *The Anatomical Record* 1968; **161**:377–392.
59. Ascenzi A, Baschieri P, Benvenuti A. The bending properties of single osteons. *Journal of Biomechanics* 1990; **23**:763–791.
60. Ascenzi A, Baschieri P, Benvenuti A. The torsional properties of single selected osteons. *Journal of Biomechanics* 1994; **27**:875–884.
61. Caputo M. *Elasticità e Dissipazione*. Zanichelli: Bologna, 1969.
62. Caputo M, Mainardi F. Linear models of dissipation in anelastic solids. *Rivista Nuovo Cimento* 1971; **II**(1):161–198.

63. Currey J. *The Mechanical Adaptations of Bones*. Princeton University Press, 1984.
64. Currey J. Physical characteristics affecting the tensile failure properties of compact bone. *Journal of Biomechanics* 1990; **30**:837–844.
65. Fung Y. *Biomechanics*. Second edition edn., Springer, 1993.
66. Heymans N. Hierarchical model for viscoelasticity: dynamic behavior in the linear range. *Rheologica Acta* 1996; .
67. Heymans N. Constitutive equations for polymer viscoelasticity derived from hierarchical models in cases of failure of time–temperature superposition. *Signal Processing* 2003; .
68. Lakes R, Katz J, Sternstein S. Viscoelastic properties of wet cortical bone - i: Torsional and biaxial studies. *Journal of Biomechanics* 1979; **12**:657–678.
69. Lakes R, Katz J. Viscoelastic properties of wet cortical bone - ii: Relaxation mechanisms. *Journal of Biomechanics* 1979; **12**:679–687.
70. Lakes R, Katz J. Viscoelastic properties of wet cortical bone - iii: Non-linear constitutive equation. *Journal of Biomechanics* 1979; **12**:689–698.
71. Lakes R. On the torsional properties of single osteons. *Journal of Biomechanics* 1995; **28**(11):1409–1410.
72. Nutting P. A new general law of deformation. *Journal of the Franklin Institute* 1921; **191**:679–685.
73. Rho J, Kuhn-Spearing L, Zioupos P. Mechanical properties and the hierarchical structure of bone. *Medical Engineering & Physics* 1998; **20**:92–102.
74. Yao H, Gao H. Mechanics of robust and releseable adhesion in biology: bottom-up designed hierarchical structure of gecko seta. *Journal of Mechanics and Physics of Solids* 2006; **54**:1120–1146.
75. Ziv V, , Wagner H, Weiner S. Microstructure-microhardness relations in parallel-fibered and lamellar bone. *Bone* 1996; **18**(5):417–428.
76. Ritchie RO, Buehler MJ, Hansma P. Plasticity and toughness in bone. *Physics Today* 2009; .
77. Ritchie RO. The conflicts between strength and toughness. *Nature Materials* 2011; **10**:817–822.
78. Weiner S, Traub W. Bone structure: from angstrom to microns. *The FASEB Journal* 1992; **6**:879–885.
79. Weiner S, Wagner H. The material bone: Structure-mechanical function relations. *Annual Review of Materials Research* 1998; **28**:271–298.
80. Bagley R, Torvik P. Fractional calculus - a different approach to the analysis of viscoelastically damped structures. *The American Institute of Aeronautics and Astronautics Journal* 1983; **21**(5):741–748.
81. Bagley R, Torvik P. A theoretical basis for the application of fractional calculus to viscoelasticity. *Journal of Rheology* 1983; **27**:201–210.
82. Bagley R, Torvik P. On the appearance of the fractional derivative in the behavior of real materials. *Journal of Applied Mechanics* 1984; **51**(2):294–298.
83. Bagley R, Torvik P. On the fractional calculus model of viscoelastic behavior. *Journal of Rheology* 1986; **30**(1):135–155.
84. Hilfer R. *Application of Fractional Calculus in Physics*. World Scientific: Singapore, 2000.
85. Liu J, Xu M. Study on the viscoelasticity of cancellous bone based on higher-order fractional models. *Bioinformatic and Biomedical Engineering* 2008; :1733–1736.
86. Schiessel H, Blumen A. Hierarchical analogues to fractional relaxation equations. *Journal of Physics A: Mathematical and Theoretical* 1993; **26**:5057–5069.
87. Schiessel R H Metzler, Blumen A, Nonnenmacher T. Generalized viscoelastic model. *Journal of Physics A: Mathematical and Theoretical* 1995; **28**:6567–6584.
88. Spanos PD, Evangelatos GI. esponse of a non-linear sys- tem with restoring forces governed by fractional derivatives-time domain simulation and statistical linearization solution. *Soil Dynamics and Earthquake Engineering* September 2010; **30**(9):811–821.
89. Tarasov VE. *Fractional Dynamics: Applications of Fractional Calculus to Dynamics of Particles*. Fields and Media Springer., 2010.
90. Yuan L, Agrawal OP. A numerical scheme for dynamic system containing fractional derivatives. *Journal of Vibration and Acoustic* 2002; **124**(2):321–324.
91. Oldham K, Spanier J. *The Fractional Calculus*. Academic Press, 1974.
92. Mandelbrot B. *The Fractal Geometry of Nature*. W. H. Freeman & Co, 1982.
93. Lasota A, Mackey M. *Chaos, Fractals and Noise. Stochastic aspects of dynamics*. Springer, 1994.
94. Mandelbrot B. *Fractals and scaling in finance. Discontinuity, concentration, risk.* Springer, 1997.
95. Falkoner K. *Fractal Geometry: Mathematical Foundetion and Application*. John Wiley & Sons: Chicester, 1990.
96. Hausdorff F. Dimension und äusseres mass. *Mathematische Annalen* 1918; **19**(1-2):157–179.
97. Minkowski H. Jahresberichte der deutschen mathematiker 1908; .
98. Bouligand G. *Sur la notion d'ordre de misure d'un ensemble plan*. 1929.
99. Kolmogorov A. Zur topologischruppentheoretischen begründung der geometrie 1930; .
100. Cuyt A, Brevik Petersen V, Verdonk B, Waadeland H, Jones W. *Handbook of Continued Fractions for Special Function*. Springer, 2008.




DOI: 10.1002/cnm